ACS NANO

www.acsnano.org

ARTICLE

Macro- and Microstructural Evolution during Drying of Regenerated Cellulose Beads

Hailong Li,* Margarita Kruteva, Katarzyna Mystek, Martin Dulle, Wenhai Ji, Torbjörn Pettersson, and Lars Wågberg*

Cite This: *ACS Nano* 2020, 14, 6774–6784

Read Online

ACCESS | Metrics & More | Article Recommendations | Supporting Information

ABSTRACT: The macro- and microstructural evolution of water swollen and ethanol swollen regenerated cellulose gel beads have been determined during drying by optical microscopy combined with analytical balance measurements, small-angle X-ray scattering (SAXS), and wide-angle X-ray scattering (WAXS). Two characteristic length scales, which are related to the molecular dimension of cellulose monomer and elongated aggregates of these monomers, could be identified for both types of beads by SAXS. For ethanol swollen beads, only small changes to the structures were detected in both the SAXS and WAXS measurements during the entire drying process. However, the drying of cellulose from water follows a more complex process when compared to drying from ethanol. As water swollen beads dried, they went through a structural transition where elongated structures changed to spherical structures and their dimensions increased from 3.6 to 13.5 nm. After complete drying from water, the nanostructures were characterized as a combination of rodlike structures with an approximate size of cellulose monomers (0.5 nm), and spherical aggregates (13.5 nm) without any indication of heterogeneous meso- or microporosity. In addition, WAXS shows that cellulose II hydrate structure appears and transforms to cellulose II during water evaporation, however it is not possible to determine the degree of crystallinity of the beads from the present measurements. This work sheds lights on the structural changes that occur within regenerated cellulose materials during drying and can aid in the design and application of cellulosic materials as fibers, adhesives, and membranes.

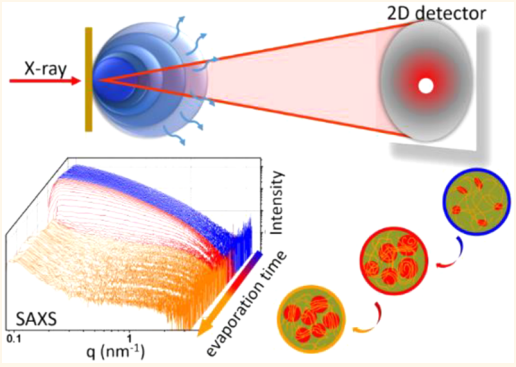

KEYWORDS: *cellulose, gel bead, drying, structural evolution, X-ray scattering*

Cellulose is one of the world's most abundant, renewable, and biodegradable polymers that is commonly extracted from wood, cotton, and so forth. It has been used as an engineering material for thousands of years, benefiting from a hierarchical structural design that spans from the molecular to macroscopic scale.[1,2] With the development of our modern circular economy, high-performance cellulose-based products are in high demand for use as high tenacity rayon,[3,4] transparent films,[5−7] hydrogels and aerogels,[8−10] microspheres and beads,[11] and so forth. Many of these products are shaped during the regeneration of the dissolved cellulose polymer.[12] It is common knowledge that cellulose cannot be melted or dissolved in water or in common organic solvents without being chemically modified. However, several solvent systems have been discovered that can dissolve cellulose without changing its chemistry. These include but are not limited to lithium chloride in *N*,*N*-dimethylacetamide (LiCl/DMAc), ionic liquids, *N*-methylmorpholine *N*-oxide, superphosphoric acid, transition metal complexes in water, and cold NaOH/urea aqueous solution.[13,14]

McCormik *et al.*[15] introduced LiCl/DMAc as a nonderivatizing solvent for cellulose in the early 1980s and since then it has become the standard solvent for gel permeation chromatography (GPC) analysis of the molecular mass of cellulosic materials.[16,17] The mechanism of cellulose dissolution in this solvent system has been studied by using nuclear magnetic resonance (NMR),[15,18,19] and it was found that LiCl/DMAc breaks the intermolecular interactions resulting in a molecular solution of cellulose. Previous work has focused on the cellulose dissolution mechanism.[20,21] There are a few recent

Received: January 7, 2020
Accepted: May 8, 2020
Published: May 8, 2020

https://dx.doi.org/10.1021/acsnano.0c00171
ACS Nano 2020, 14, 6774–6784

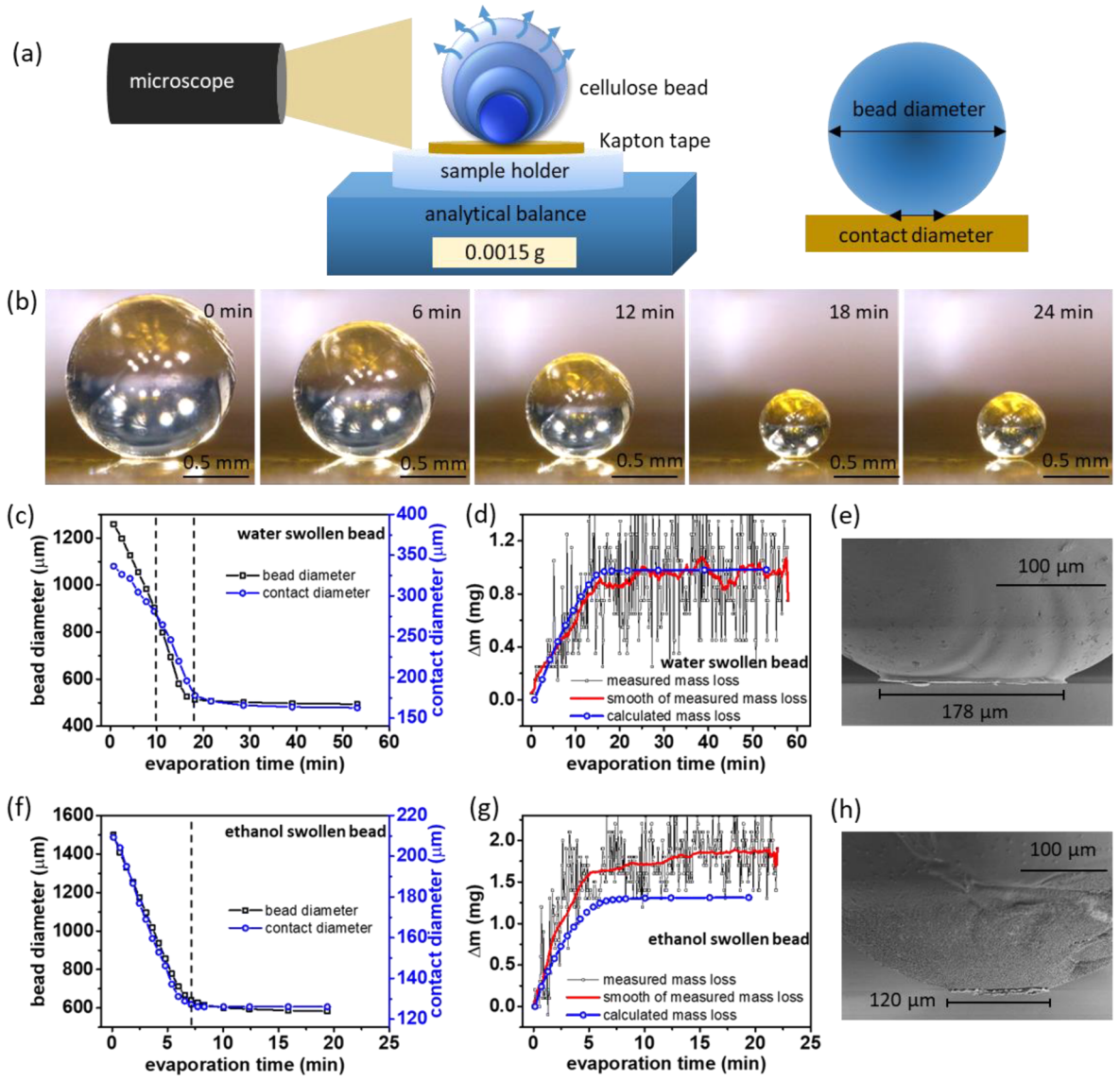

Figure 1. (a) Schematic illustration of the *in situ* optical microscopy measurements of swollen beads during drying. (b) Side-view images of the drying of a water swollen bead on the Kapton tape at 22 °C and 28% ± 2% relative humidity (RH). Representative diameter (black squares) and contact diameter (blue circles) of (c) water swollen and (f) ethanol swollen beads measured from the side-view images. The measured Δm (black open squares) and calculated mass loss Δm_{calc} (blue open circles) of (d) water swollen and (g) ethanol swollen beads during drying; the red curve is the smoothed curve of the measured mass loss. SEM images of the contact zone (between the bead and the Kapton tape) of the dried (e) water swollen and (h) ethanol swollen beads after 2 days of drying.

studies where the supramolecular rearrangements in cellulose thin films were established by grazing incidence small-angle X-ray scattering (GISAXS) measurements during the conversion of trimethylsilyl cellulose to cellulose *via* HCl vapor hydrolysis,[22,23] and the effect of heat treatment on its structure and morphology was established.[24] GISAX was also employed by Roth *et al.* to characterize the structure of spray-deposited nanocellulose thin film and the water-induced structural rearrangements during drying.[25,26] However, the molecular arrangement of dissolved cellulose during the regeneration process it is still not fully established and it is not clarified how the dissolved cellulose molecules are affected by changes in, for example, temperature, pressure, and/or the uptake/release of molecules during regeneration. A thorough understanding of these mechanisms would be essential for the preparation of cellulose-based materials, such as fibers, membranes and adhesives.

Recently, we have successfully prepared macroscopic cellulose gel beads by precipitating cellulose/LiCl/DMAc solutions into a nonsolvent (ethanol or water).[27−30] These beads have been used as models to investigate the swelling behavior of the wet, delignified cellulosic fibers of wood.[28] These nanometer smooth dried cellulose beads have also been used as probes to conduct contact adhesion measurements between cellulose and other materials.[27,30] NMR and SAXS measurements of the beads in the wet state indicate that the internal structure of macroscopic cellulose gel beads can be considered as a microgel system whereby the cellulose forms a homogeneous, noncrystalline, and molecularly dispersed polymer network.[28,29] Many studies have been conducted to elucidate the equilibrium structures of a variety of microgel systems with different chemistries in swollen or collapsed states.[31−41] Kinetic studies of the structural response of swelling[42−45] and deswelling[46−48] microgels have been

https://dx.doi.org/10.1021/acsnano.0c00171
ACS Nano 2020, 14, 6774−6784

reported. However, there are few studies investigating the kinetics of microstructure changes within microgel beads during drying.[49] Evaluating the micro- and macrostructural changes of cellulose is, for example, also very important when considering using cellulose beads to study how cellulose surfaces consolidate toward each other or toward other materials during the drying of cellulose-rich materials or in fiber-reinforced composites.

In the present work, cellulose beads were prepared from dissolved cellulose LiCl/DMAc solution by precipitating droplets of a controlled size in a nonsolvent; the beads were then divided into two fractions: one fraction was solvent exchanged to water (water swollen beads) and the others solvent exchanged to ethanol (ethanol swollen beads). The macroscopic changes of these two types of cellulose beads during solvent evaporation were evaluated by optical microscopy while drying on an analytical balance, as outlined in Figure 1a. The bead size, contact diameter, and weight were recorded throughout the solvent evaporation process. *In situ* SAXS/WAXS kinetic measurements on both types of cellulose beads were then conducted to follow the nano/microstructural evolution during drying.

RESULTS AND DISCUSSION

Microscopic Characterization of the Cellulose Gel Beads during Drying. Figure 1b shows representative side-view optical microscopy images of water swollen cellulose beads during drying. The bead size decreased with increased evaporation time, while the bead retained its spherical shape. From the quantitative values of bead diameter and contact diameter, presented in Figure 1c, it is clear that the bead diameter of water swollen beads decreased from 1260 to 520 μm during the first 17 min, after which the diameter remained constant with increasing evaporation time. However, the contact diameter of the water swollen beads decreased from 335 to 275 μm in the first 10 min, then decreased more quickly to 180 μm over the next 7 min from which point it stayed constant. The SEM image (Figure 1e) shows a final contact diameter of around 178 μm. For ethanol swollen beads, the bead diameter decreased continuously from 1500 to 615 μm for 7 min and then remained constant (see Figure 1f). The contact diameter has a similar trend, decreasing from 210 to 125 μm in 7 min. The SEM image (Figure 1h) of the final contact diameter is approximately 120 μm.

The mass loss (Δm) for water and ethanol swollen beads obtained during the drying are plotted in Figure 1d,g, respectively. The red curves are the smoothened line plots of the measured Δm. The Δm for water swollen beads increased to 1.0 mg over 17 min of evaporation and then fluctuated slightly around 1.0 mg. However, for ethanol swollen beads the Δm increased to 1.6 mg after 7 min and then increased slowly to 1.8 mg. This value is almost two times higher than the value measured for water swollen beads, which indicates that some water molecules are trapped inside the water swollen beads even after drying for 60 min. From the side-view optical microscopy images, we can determine that that both water and ethanol swollen beads shrink homogeneously and retain their spherical shape. If we assume that there are no cavities or empty pores inside the beads during the entire drying process, the mass losses of the beads can be calculated using the following formula

$$\Delta m_{calc} = m_0 - m = \frac{1}{6}\rho\pi(d_0^3 - d^3) \quad (1)$$

where d_0 is the initial swollen diameter and d is the diameter during drying, which is shown in Figure 1c,f. Using the density of water (1.00 mg/mm^3) and ethanol (0.789 mg/mm^3), the Δm_{calc} of water swollen and ethanol swollen cellulose beads were calculated for the drying process and plotted as blue open circles in Figure 1d,g, respectively. Surprisingly, the Δm_{calc} for water swollen beads almost overlaps the measured Δm throughout the drying process. However, the Δm_{calc} for ethanol swollen beads is much lower than the measured value. The difference between the measured and the calculated Δm increases with evaporation time. The apparent dry densities (calculated from the mass and the size of the dry beads) for water swollen and ethanol swollen beads are 1.40 and 0.85 g/cm^3, respectively. Therefore, the assumption that no cavities or empty pores are formed inside the beads during the entire drying process is true for water swollen beads but most likely incorrect for ethanol swollen beads.

This finding is further supported by the measured transparency changes for these two types of beads during drying (see Figure S1 in the Supporting Information). For water swollen beads, the transparency remains constant after drying for 14 min. However, the transparency of ethanol swollen beads starts to decrease after 7 min and decreases further with increased evaporation time. This is likely due to the multireflection and scattering of light inside the drying ethanol swollen beads, which result from heterogeneities within the sample such as pores and other light scattering structures.

Morphologies of Cellulose Wet and Dry Beads. In order to further characterize the internal morphologies of the wet beads, critical point drying (CPD) was used. This procedure allows for the preparation of samples for SEM characterization with a preserved wet structure, as the capillary forces (exerted on the wet structure by the evaporation liquids) can nearly be eliminated.[50] Detailed information on the CPD sample preparation can be found in the SI. The SEM images of CPD samples for water and ethanol swollen cellulose beads are shown in Figure 2a,c, respectively. The images clearly show an open, fibrous, 3D cellulose network and empty pores within both swollen beads.

The morphologies of the interior of the beads dried through ambient pressure drying are shown in Figure 2b,d. Figure 2b′,d′ are magnifications of the red dashed boxes in Figure 2b,d, respectively. Two main phenomena are observed from these SEM images: first, the fibrous network in water swollen beads (Figure 2a) seems to collapse to form spherical-like structures (Figure 2b′) after drying. Second, the fibrous structure in ethanol swollen beads is retained even after the ethanol has evaporated (Figure 2d′). These two phenomena are consistent with both the optical microscopy and transparency measurements that predicted that there are pores inside the dried, and drying, ethanol swollen beads and no pores inside water swollen beads.

SAXS Characterization of the Cellulose Gel Beads during Drying. As a complement to the macrostructure evaluation, the nano/microstructural evolution during the drying process was evaluated by SAXS (Figure 3 and Figure S3). The time-resolved SAXS curves were corrected for the use of Kapton tape and the results are summarized in Figure 3c,d for the water swollen and ethanol swollen beads, respectively.

https://dx.doi.org/10.1021/acsnano.0c00171
ACS Nano 2020, 14, 6774−6784

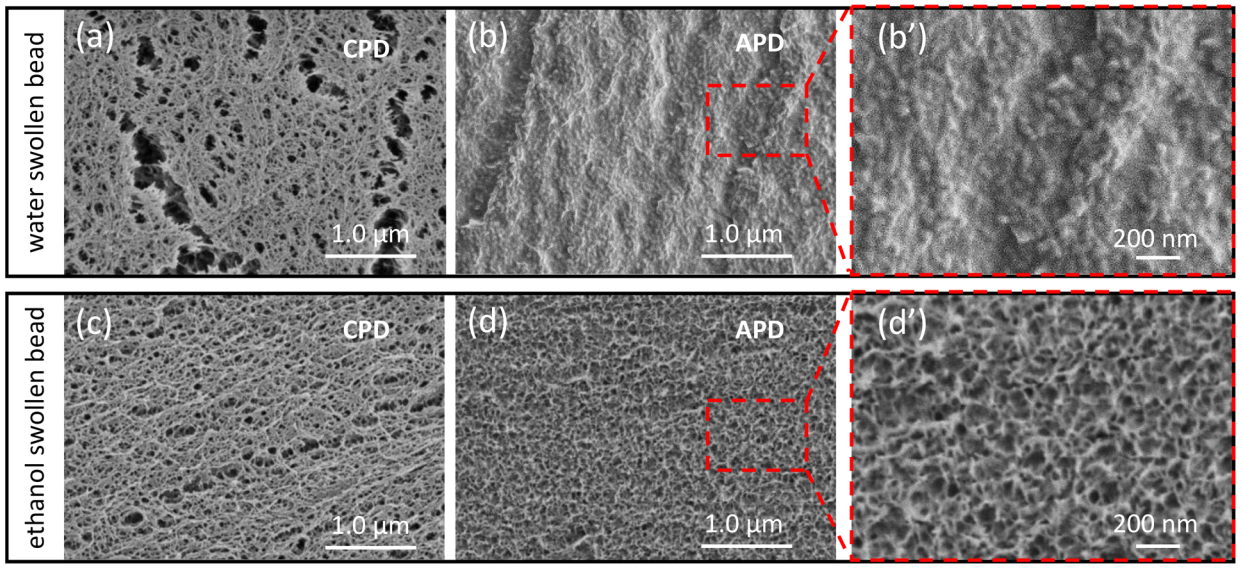

Figure 2. SEM images of (a) water swollen and (c) ethanol swollen cellulose beads dried by CPD. SEM images of (b) and (d) are of APD water swollen and ethanol swollen cellulose beads, respectively. (b′,d′) Magnifications of the red dash boxes in (b,d), respectively.

The shape of the SAXS curves for the ethanol swollen beads only change slightly during the entire drying process, indicating that the internal structure did not change significantly. However, the situation is much more complicated for the water swollen beads, whereby three regimes can be assigned to the drying sequence based on the shape of the SAXS curves. In the first regime (regime I, Figure 3c), the shape of SAXS curve does not change significantly, similar to the case for the ethanol swollen beads. However, when transitioning to regime II, after around 18 min, the intensity in the low-q region (below 0.8 nm^{-1}) decreases rapidly with time. In the high-q region (above 0.8 nm^{-1}), which corresponds to the local structure inside of the beads, it is also possible to detect a change in the shape of the curves. After 28 min, the scattered intensity again becomes constant over the entire q-region which can be defined as the start of the regime III. In this regime, the intensity in the lower-q region (below 0.2 nm^{-1}) remains higher than in the other regions and there is only a modest change in the shape of the curves with increasing evaporation time.

To quantitatively evaluate the structural changes of the water and ethanol swollen beads the Guinier-Porod model was used to analyze all SAXS curves.[51] The fitting details are summarized in the SI (*e.g.*, the six fitting parameters used are R_{g1}, R_{g2}, s_1, s_2, α, and β). This model assumes two characteristic length scales in the system defined as R_{g1} and R_{g2}. Additionally, the "dimensionality" parameters s_1 and s_2 are used to characterize the shape of the corresponding scattering objects. In general, for scattering objects with spherical symmetry $s_1 = s_2 = 0$ and for cylindrical objects $s_1 = 1$ and $s_2 = 0$. For lamellae with equal width and length, the values are $s_1 = 2$ and $s_2 = 0$. The microscopic structure of the cellulose beads is more complicated than single geometrical objects, therefore we suggest it is represented by a combination of the above-mentioned structures. The quality of the fitting is good and is presented in Figure 3b for data measured after drying water swollen beads for 5, 25, and 50 min.

The change of the characteristic length scales from the SAXS measurements, R_{g1} and R_{g2}, as a function of the drying time is shown in Figure 3e,f for water swollen and ethanol swollen beads, respectively. For water swollen beads, the value for R_{g1} decreases slightly from 0.75 to 0.65 nm during the first 18 min (regime I, Figure 3e) and then increases to 1.2 nm during the next 10 min (regime II, Figure 3e), after which it decreases to a constant level of approximately 0.5 nm after 45 min. The value for R_{g2} increases from 2.8 to 3.6 nm in the first 18 min after which it rapidly increases to 13.5 nm after 32 min drying. After this phase, R_{g2} continues to increase but at a much lower rate. Because of the fast evaporation rate of ethanol, the drying process for ethanol swollen beads is more rapid. Figure 3f shows that the changes of the R_{g1} and R_{g2} values for beads dried from ethanol follow distinctly different pathways as a function of evaporation time compared to those dried from water. R_{g1} decreases from 0.85 to 0.60 nm during the first 8 min, then stays constant at 0.60 nm. R_{g2} increases from 2.2 to 2.8 nm in 8 min, then slowly decreases to 2.3 nm. This indicates that the structure of ethanol swollen beads does not change significantly during the evaporation process. Interestingly, Ishii *et al.* found similar length scales for a water-coagulated cellulose gel prepared by dropping distilled water into the cellulose/LiCl/DMAc solution.[52] They proposed that the smaller scale length (less than 1 nm) reflected the distance between the nearest neighboring chains in the network and the larger scale length (roughly 6 nm) is likely related to larger structures, that is, the entanglement of cellulose molecules dissolved in LiCl/DMAc.[52,53] From the order of magnitude and basic knowledge of cellulose microstructure, we can relate R_{g1} to the size of cellulose monomer (as it is in the size range of the anhydroglucose unit) and R_{g2} can be used to characterize the size of the elongated aggregate structures or persistent length of cellulose strands inside both the water swollen and ethanol swollen cellulose gel beads.

The values of the "dimensionality" parameters, s_1 and s_2, as a function of the drying time are shown in Figure 3g,h for water swollen and ethanol swollen beads, respectively. For water swollen beads, the value for s_1 remains near 2 over the first 18 min (regime I, Figure 3g) and then decreases rapidly to 0 during the next 10 min (regime II, Figure 3g), after which it increases slowly to 0.5 after 45 min. The value for s_2 decreases from 1.2 to 0.8 in regime I and then continues to decrease at an accelerated rate to 0 in regime II. After this phase, the s_2

https://dx.doi.org/10.1021/acsnano.0c00171
ACS Nano 2020, 14, 6774−6784

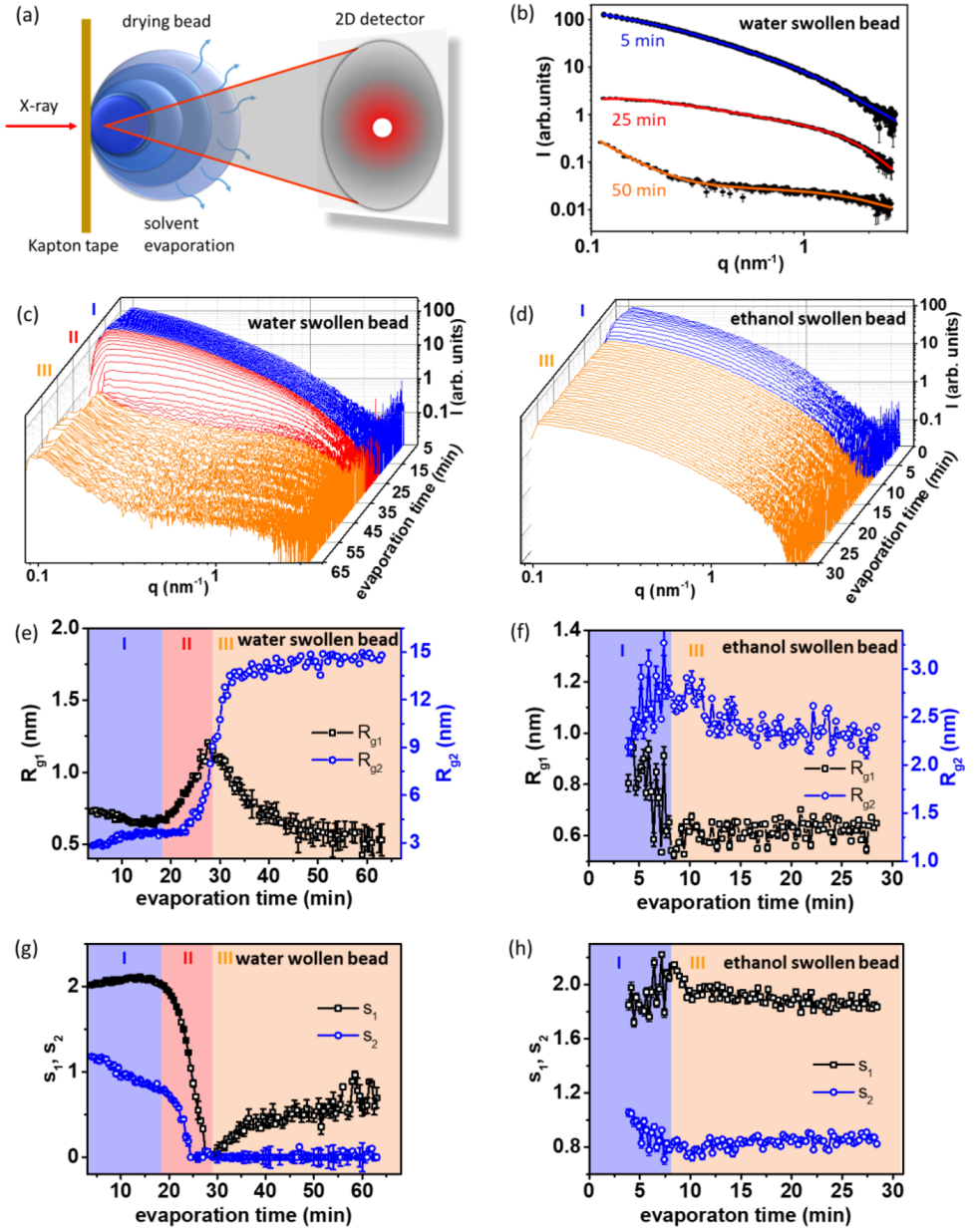

Figure 3. (a) Schematic illustration of the *in situ* SAXS/WAXS measurements during the drying of the wet beads at 26 °C and 33% ± 2% RH. As schematically shown in panel a, the X-ray beam passes through the center of beads and scatters toward the 2D detector. (b) SAXS data for the water swollen bead after drying for 5, 25, and 50 min (black points) and the corresponding fitting curves in blue, red, and orange. (c) The whole SAXS data set for the water swollen bead over a time span of 60 min with a time step between each curve of 30 s. (d) The entire SAXS data set for the ethanol swollen bead over a time span of 30 min with a time step between each curve of 15 s. Time-dependent changes caused by evaporation for the two fitted length scales parameters (R_{g1} and R_{g2}) for (e) water swollen and (f) ethanol swollen beads during the drying process. Time-dependent changes due to evaporation for the "dimensionality" parameters (s_1 and s_2) for (g) water swollen and (h) ethanol swollen beads during the drying process.

stays constant at 0. However, for ethanol swollen beads, s_1 and s_2 remain near 2 and 0.8, respectively, during the entire drying process, indicating that the shapes of the corresponding two structures do not change significantly during the evaporation process. A detailed discussion of the nanoscale structural changes that occur during drying is presented below.

WAXS Characterization of the Cellulose Gel Beads during Drying. To investigate whether crystalline order is developed during the drying process, WAXS measurements were conducted under the same conditions as those used for the SAXS measurements. The data extraction was performed in a similar way to that for SAXS data. Representative WAXS curves for the entire drying process are summarized in Figure 4a,b for water swollen and ethanol swollen beads, respectively. For water swollen beads, the scattering peak from water, around q = 20.0 nm^{-1},[54] and that from cellulose, at q = 14.6 nm^{-1},[55,56] are present throughout the entire drying process. Another weak and broad scattering peak at q = 8.0 nm^{-1} appears from the beginning of regime II (18 min) and shifts to higher q = 8.8 nm^{-1} at the end of regime II, after which it continues to shift to a q value of around 9.4 nm^{-1} in the later phase of the drying (Figure 4a′).[57,58] Values of 2θ = 12.4° and 20.6° assigned to $(1\bar{1}0)$ and (110) crystallographic planes of the cellulose II structure were calculated from the equation

https://dx.doi.org/10.1021/acsnano.0c00171
ACS Nano 2020, 14, 6774−6784

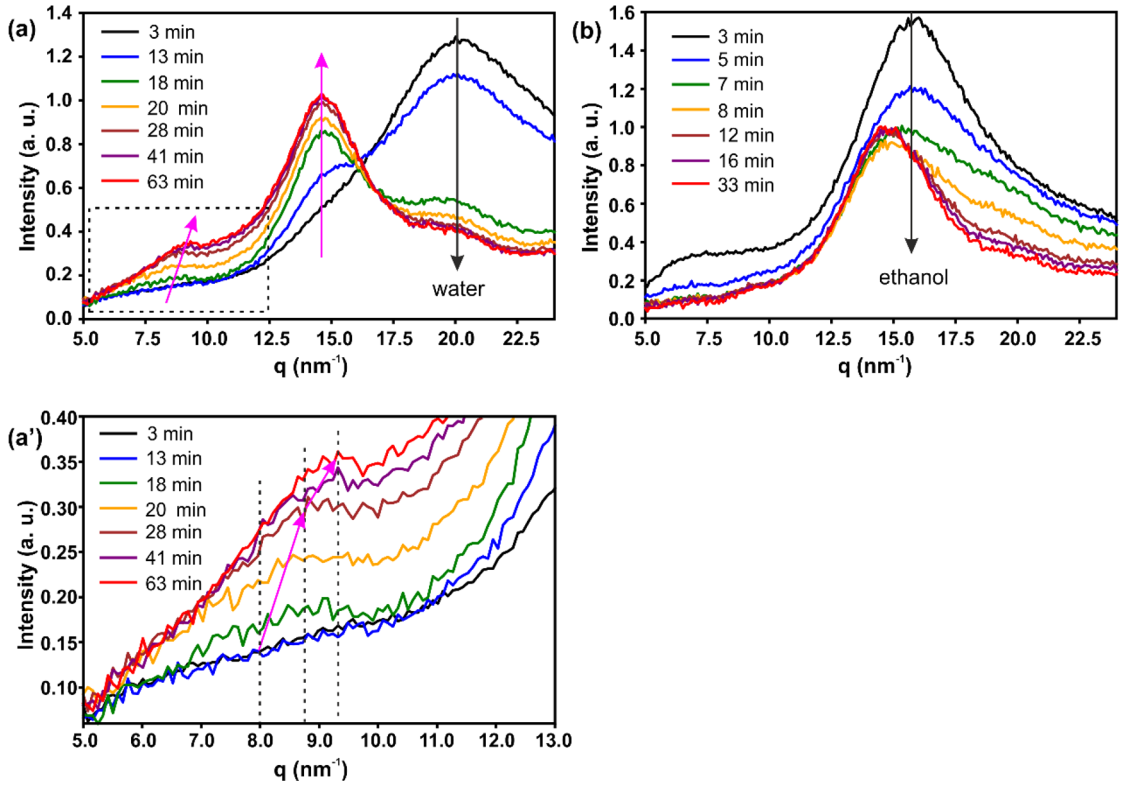

Figure 4. Representative WAXS curves for (a) water swollen and (b) ethanol swollen beads after drying for different times at 26 °C and 33% ± 2% relative humidity. Each curve was measured at 30 or 15 s intervals for water swollen and ethanol swollen beads, respectively. (a′) Magnification of the black dashed box in (a).

$q = \frac{4\pi \sin\theta}{\lambda}$ for q = 8.8 and 14.6 nm^{-1} using λ = 0.154 nm.[55,56,59,60] The phenomenon of peak shifting along the [1$\bar{1}$0] direction (from 8.0 to 8.8 nm^{-1}) has been observed for mercerized cellulose II fibers by Wada *et al.*[57,58] They proposed that a slightly expanded cellulose II hydrate structure changes to a cellulose II structure after drying. Thus, we suggest that a cellulose II hydrate structure forms at the beginning of regime II and transitions to a cellulose II structure continuously in this drying regime. However, currently it is not possible to determine the degree of crystallinity of the beads from the present measurements due to the strong scattering of solvents and the difficulty of identifying the amorphous background. Previous solid state NMR measurements of similarly produced cellulose beads[28] have shown a very low degree of crystallinity and we therefore postulate that our beads have a similarly low degree of crystallinity. For ethanol swollen beads, except for the intensity change of both the ethanol scattering peak (at q = 15.5 nm^{-1})[61] and the cellulose scattering peak (at q = 14.6 nm^{-1}), no crystalline cellulose diffraction peaks are observed in the WAXS curves (Figure 4b). This indicates that no crystalline structures are formed during drying from ethanol swollen beads, which is consistent with the SAXS results.

Structural Evolution on Different Hierarchical Levels during Drying. Results from the optical microscopy and analytical balance measurements, SEM, SAXS, and WAXS measurements, relating to macro- structure, morphology, and micro- structure, have all been shown separately in earlier sections. In order to develop a unified description of the internal structure of the cellulose beads and how this structure changes during drying, it is necessary to combine the results from all these different measurements. This section will be devoted to the analysis and discussion of both the macro- and microstructural evolution of cellulose during the entire drying process.

Internal Structure of the Cellulose Beads in Swollen State. It is well-known that cellulose has a rigid molecular chain that does not fold easily to form ordered crystalline structures in concentrated gels. This is supported by the WAXS curves obtained in the early drying regime for both water swollen and ethanol swollen beads (black curves in Figure 4a,b), where no diffraction peaks for the cellulose crystalline structure were observed. However, a small peak at q = 14.6 nm^{-1}, hidden beneath both the water and ethanol scattering peak, is observed, which indicates the presence of small amounts of local aggregate structures inside the gel beads. These results support the use of the two characteristic length scales (R_{g1} and R_{g2}) to fit the SAXS data. Before the drying starts, the fitted value of s_1 is approximately 2 and s_2 is around 1 for both water and ethanol swollen beads. This indicates that there might be a lamellar-like stacking of the cellulose monomers (s_1 = 2) with a size on the order of 1 nm (yellow region in Figure 5) combined with larger elongated structures (red region in Figure 5). The longest dimension of this elongated object cannot be exactly determined but the shortest size related to R_{g2} is approximately 3 nm. It could be suggested that the strong interactions between cellulose molecules is the driving force for the association of the molecules and the formation of an aggregated structure that is linked by long segments of cellulose chains forming the final 3D network. This agrees with the physical structure as suggested in our previous work, where a noncrystalline polymer network structure was proposed for the cellulose gel beads.[28,29]

https://dx.doi.org/10.1021/acsnano.0c00171
ACS Nano 2020, 14, 6774−6784

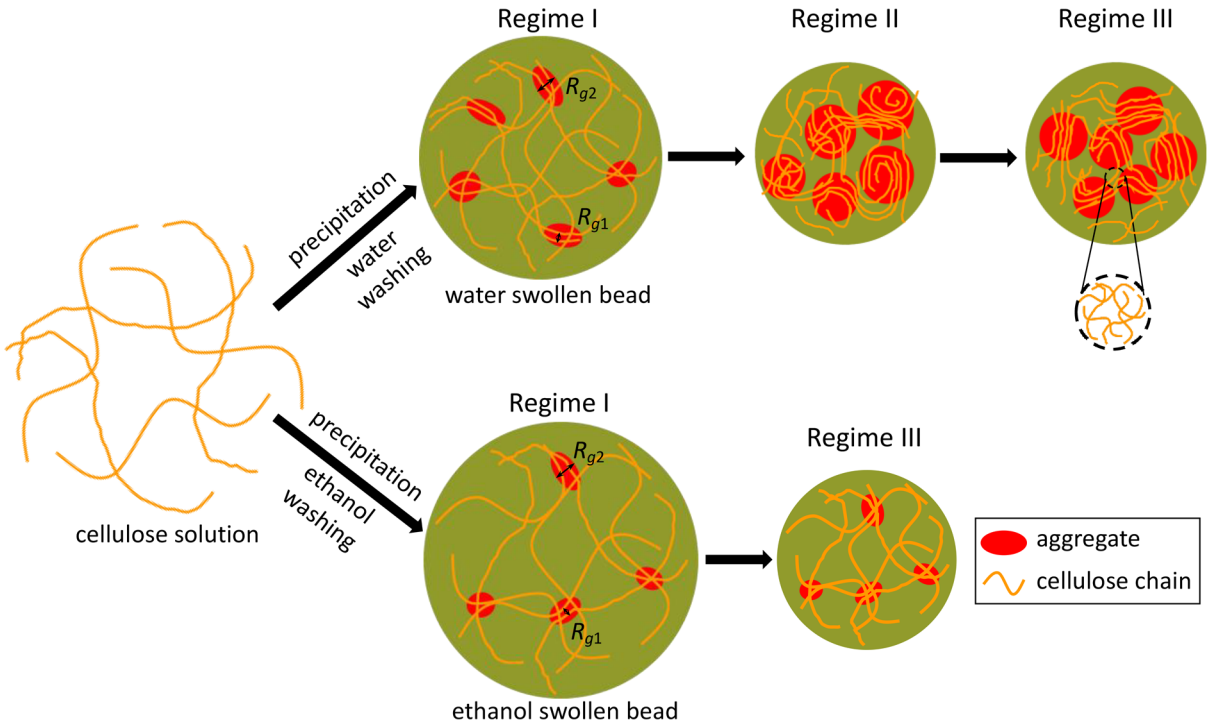

Figure 5. Schematic representation of the structural evolutions of the water swollen and ethanol swollen cellulose beads during solvent evaporation.

Interestingly, at evaporation time t = 0, the initial cellulose aggregate size R_{g2} inside water swollen beads (2.8 nm) is larger than the aggregates found inside ethanol swollen beads (2.2 nm), even though the interaction between cellulose and water is stronger than the interaction between cellulose and ethanol. The most probable explanation for this is that cellulose chains, which are in a fully dissolved state in the cellulose/DMAc/LiCl solution, form small aggregated structures locally during the washing and removal of DMAc/LiCl. Specifically, LiCl has a higher solubility in water than in ethanol at room temperature,[62] which suggests that LiCl will be more readily removed from the beads by water. This will likely result in larger aggregates inside water swollen beads. The shrinking of the swollen beads is a consequence of the formation of these aggregates and it can be suggested that the larger the aggregates, the larger the degree of shrinking of the swollen beads will be. This can be seen by the fact that the initial diameter of water swollen beads (1260 μm) is much smaller than the ethanol swollen beads (1500 μm) (Figure 1c,f).

Macro- and Microstructural Evolution during Drying. Because of the loose packing of the cellulose chains in the swollen beads (resulting from the low cellulose concentration), the dimension of the beads can change significantly with evaporation time (Figure 1c,f). For the water swollen beads in regime I (Figure 3g), s_1 stays around 2, and s_2 continuously decreases from 1.2 to 0.8. This indicates that the internal local structure does not change significantly. However, the characteristic length R_{g1} decreases as the bead shrinks during solvent evaporation (Figure 3e). At the same time, the characteristic length R_{g2} slightly increases, which demonstrates a progressive aggregation process. It is important to note that in the swollen state and, specifically, in regime I the structure of cellulose in water and in ethanol is very similar, demonstrating a simultaneous existence of monomer stacking and larger elongated structures (Figure 5).

For the drying of water swollen beads in regime II (Figure 3g), s_1 and s_2 rapidly decrease to 0 indicating the formation of structures with spherical symmetries (see above, s_1 = 0 and s_2 = 0). From Figure 3e, it can be noted that R_{g2} increases to 9 nm during this interval. As previously calculated by Bertrand *et al.*[63] there is an effective tensile stress exerted on a polymer network of an ideal elastomeric gel during free drying. We propose that the existing aggregates will be pulled together by this tensile stress, induced by drying, to form larger spherical structures. The unexpected increase of R_{g1} in this regime is proposed to be due to the extra space between the aggregate structures that is created when these structures merge into larger structures. It is worth mentioning that the cellulose II hydrate structure appears and transitions into cellulose II during this drying phase (Figure 4a), although it is currently not possible to determine the degree of crystallinity of the beads. On the basis of the SAXS and WAXS data in regime II it is clear that the cellulose chains merge into larger structures with a spherical symmetry. Meanwhile, some cellulose chains inside the spherical aggregates start to form cellulose II hydrate which changes to cellulose II during this drying phase. This sharp structural transition leads to a concentration gradient of cellulose chains on the aggregate surface, which is supported by obtaining a Porod exponent α-value in the range of 5−6 (Figure S4a). This phenomenon can also explain why the bead diameter decreases more rapidly in regime II, Figure 1c. For ethanol swollen beads this process is not observed.

In regime III (Figure 3g), s_1 increases slowly to approximately 0.5 for water swollen beads. In comparison to the lamellar-like stacking of the cellulose monomers observed in the regime I, the objects with smaller characteristic sizes tend to form rodlike structures with an approximate size equivalent to that of a cellulose monomer (0.5 nm) in regime III. This structural evolution is likely caused by the release of the tensile stress, induced during the previous fast collapse

https://dx.doi.org/10.1021/acsnano.0c00171
ACS Nano 2020, 14, 6774−6784

process (regime II). Because of the presence of water molecules trapped inside the beads, as indicated from the earlier results (Figure 1d,g, and 4a), cellulose chains are still mobile enough to change their conformation. Such conformational rearrangements result in the release of the tensile stress. This type of stress release has been supported by the theoretical calculations[63] for elastomeric gels during the late stages of drying, similar to regime III in the present work. A consequence of the conformational change is the decrease of R_{g1} from 1.2 to 0.5 nm (regime III in Figure 3e). This value is close to the initial value of 0.7 nm in the swollen state. A similar decrease is observed for the d-spacing of the $(1\bar{1}0)$ plane, where the q shifts from 8.8 to 9.4 nm^{-1} in regime III (see Figure 4a′). According to equation: $d = \frac{2\pi}{q}$, $d_{(1\bar{1}0)}$ decreases from 0.714 to 0.668 nm. R_{g2} stays constant or shows a slight increase in this regime. First of all, the diameter and water content of the water swollen beads in regime III are almost constant (Figure 1c,d). Second, for water swollen beads at longer drying time the scattering patterns are covered by the Porod scattering in the low Q-regime (see Figure 3c). Therefore, the uncertainty for the R_{g2} is slightly increased due to limited interval of the available q-range. However, the larger objects maintain a spherical symmetry ($s_2 = 0$). This suggests that the stress release does not change the shape of the larger objects, which leads to the conclusion that the bead diameter does not decrease in the later drying phase in Figure 1c,f. On the basis of these results, we suggest that the residual stress is slowly released in regime III *via* conformational change of cellulose chains which results in an increase of s_1 and the decrease of R_{g1}. Finally, large spherical-like aggregates with rodlike cellulose chains inside are formed in the beads after 1 h of drying from water. For ethanol swollen beads, s_1 and s_2 do not change significantly with evaporation time after regime I, indicating no major change of the shape of the internal structure upon drying. This suggests that the tensile stress on the network is not sufficient (due to the lower surface tension of ethanol) to deform the network structures, and hence the initial porous structure inside ethanol swollen beads will be maintained even in the dry state (Figure 2d′).

It is well established that the $I(q) \sim q^{-1}$ behavior of the scattering profile for dilute solution corresponds to a characteristic scattering pattern of rodlike structures.[64,65] This behavior is observed for the cellulose solution over a relatively broad region $q > 0.1$ nm^{-1} (red curve in Figure S5). This suggests that cellulose chains exist as rodlike rigid polymers in DMAc/LiCl on large length scales, likely due to the intramolecular interactions between the adjacent glucose segments within cellulose molecules. Similar behavior was observed by Hirosawa *et al.* by dissolving cellulose in a phosphonate-based ionic liquid.[64] Surprisingly, the $I(q) \sim q^{-1}$ behavior is also found at a much higher q-region, $q > 0.4$ nm^{-1}, for water swollen beads after 1 h of drying (black dot curve in Figure S5). This suggests that the cellulose chains in the beads drying from water have a similar rodlike conformation, on the smaller length scale, as in cellulose solution. This is consistent with the results from the fitted value of $s_1 = 0.5$ in regime II (Figure 3g).

CONCLUSION

In conclusion, it has been demonstrated that the use of optical microscopy in combination with analytical balance and *in situ* SAXS/WAXS measurements allows for a comprehensive description of the macro- and microstructural evolution (Figure 5) of the swollen cellulose beads during drying. The change in the macroscopic bead size is related to the microstructure organization and reorganization during the solvent evaporation. Two characteristic length scales that are related to the molecular dimension of cellulose monomer (1 nm) and elongated aggregates (3 nm) were found for both water swollen and ethanol swollen cellulose beads by SAXS. However, the drying of cellulose from water follows a different process compared to the drying from ethanol. For water swollen beads, both structures show a change in their dimensions and morphology upon drying, passing through a sharp structural transition where small elongated structures transition to large spherical structures. After complete drying, water swollen beads with an initial porous polymer network structure shrink to form solid dry beads. Moreover, cellulose II hydrate was observed by WAXS at the beginning of regime II and was seen to continuously transform to cellulose II during water evaporation. For ethanol swollen beads, no major changes to the internal structure were observed from either SAXS or WAXS measurements, and a porous cellulose network was maintained throughout the drying process. These results demonstrate the different structural evolutions of ethanol swollen and water swollen cellulose gel beads. This work contributes to the understanding of the mechanisms and processes that occur during the drying of regenerated cellulose gels and potentially leads to essential improvements of the cellulose drying process.

METHODS AND EXPERIMENTAL SECTION

Materials. The raw material used to prepare the cellulose solution and cellulose gel beads was Domsjö dissolving pulp provided by Domsjö Fabriker AB, Sweden. The fibers from this dissolving pulp contain 96% glucose[28,66] and their charge density is reported as 29 μeq/g.[67] To dissolve the dissolving pulp the following chemicals were used: ethanol (EtOH, 96 vol %) purchased from VWR International AB; lithium chloride (LiCl, puriss p.a., anhydrous ≥99%), and *N*,*N*-dimethylacetamide (DMAc, puriss p.a., ≥99.5%), purchased from Sigma-Aldrich. All chemicals were used without further purification.

Preparation of Cellulose/LiCl/DMAc Solution. In order to make cellulose beads, cellulose/LiCl/DMAc solution was prepared according to the previously described protocol.[27,28,68] The pulp was pretreated by washing with deionized water to remove metal ions and dissolved colloidal substances (carbohydrates, lignin, and extractives). Water saturated pulp with a dry mass of 1.5 g was solvent-exchanged to ethanol and subsequently DMAc through multiple filtration steps. The solvent-exchange steps were performed over 2 days for each solvent with the solvent being changed at least twice each per day, using approximately 150 mL each time. After the solvent exchange, 100 mL of DMAc was heated to 105 °C for 20 min in an oil bath and 7 g of LiCl was heated in an oven at 105 °C for 30 min to release any entrapped water. The dehydrated LiCl was added to the warm DMAc and allowed to cool. When the temperature reached 65 °C the DMAc saturated pulp was added to the dehydrated DMAc/LiCl solution. After overnight stirring, a transparent 1.5 wt % cellulose solution was obtained.

Preparation of Cellulose Gel Beads. The cellulose/LiCl/DMAc solution was precipitated dropwise into a nonsolvent (ethanol, 96 vol %), where the cellulose solidified as spherical droplets. The precipitation was performed using an infusion pump (Harvard Apparatus, Holliston, MA, model PHD 2000). The prepared spherical droplets were left to equilibrate for 24 h in the precipitation bath. Next, the spheres were continuously washed with fresh Milli-Q water or 96% ethanol for at least 7 days to ensure a proper removal of the cellulose solvent. The beads were stored in Milli-Q water (water swollen beads) or 96% ethanol (ethanol swollen beads).

https://dx.doi.org/10.1021/acsnano.0c00171
ACS Nano 2020, 14, 6774−6784

CPD and Ambient Pressure Dried (APD) Drying of Cellulose Beads. In order to observe the interior morphology of water swollen and ethanol swollen beads with an SEM, CPD was used to prepare samples. The prepared water swollen and ethanol swollen cellulose beads were solvent exchanged to pure ethanol over 2 days by changing the solvent to pure ethanol three times per day. The beads were then placed in the CPD chamber (Autosamdri-815, Tousimis, U.S.A.) and liquid carbon dioxide was injected into the chamber under a pressure of about 50 bar for solvent exchange from ethanol to CO_2. The conditions of the chamber were then brought above the CO_2 critical point, to about 100 bar and 36 °C, after which the chamber was depressurized and the CO_2 evaporated. To characterize the interior morphology of beads after normal ambient drying, the water swollen and ethanol swollen beads were dried for 48 h under ambient pressure at 22 °C with 28% ± 2% RH, these have been named as the "APD" bead samples. The drying conditions were kept the same for the optical microscopy measurements.

Optical Microscope Characterization. The diameter of the wet cellulose beads, as well as the contact diameter between the cellulose beads and the substrate were monitored using an optical microscope (AM7013MZT, Dino-Lite Premier Digital Microscope). As depicted in Figure 1a, a cellulose bead was placed on the analytical balance (SAG204, Mettler Toledo), which was used to record the weight of the samples during the drying process at 22 °C with 28% ± 2% RH. Kapton tape (part number, 42-020-0016) was used as the substrate for both optical microscopy and SAXS/WAXS measurements.

Field Emission Scanning Electron Microscope (FE-SEM). The microstructures and morphologies inside the CPD and APD beads were imaged using an S-4800 field emission scanning electron microscope (FE-SEM) (Hitachi, Tokyo, Japan) instrument operating at high vacuum. CPD and APD beads were immersed in liquid nitrogen, crushed with a metal rod, air-dried, glued onto a sample holder using conductive carbon tape, and then coated with Pt/Pd in a Cressington 208 HR sputter coater (Cressington Scientific Instruments, Watford, U.K.) for 20 s to reduce specimen charging during the SEM imaging.

Small-Angle/Wide-Angle X-ray Scattering (SAXS/WAXS). *In situ* SAXS/WAXS measurements of the drying of wet cellulose beads are depicted in Figure 3a. The scattering patterns were recorded with the SAXS system "Ganesha-Air" from SAXSLAB/XENOCS. The X-ray source of this laboratory based system is a D2-MetalJet (Excillum) with a liquid metal anode operating at 70 kV and 3.57 mA with Ga–K_α radiation (wavelength λ = 0.1314 nm), providing a very brilliant and a very narrow beam (<100 μm). The beam was further focused with a focal length of 55 cm, using a specially made X-ray optics (Xenocs) to provide a very narrow and intense beam at the sample position. Two pairs of scatterless slits were used to adjust the beam size depending on the detector distance. The data were acquired with a position-sensitive detector (PILATUS 300 K, Dectris). After calibration with silver behenate, the distance from the sample to the detector was set to 1107 and 152 mm relating to a q-range 0.08 $nm^{-1} \leq q \leq 3.5$ nm^{-1} and 5.0 $nm^{-1} \leq q \leq 24.0$ nm^{-1} for SAXS and WAXS measurements, respectively. Here q is the magnitude of the scattering wave vector defined as $q = \left(\frac{4\pi}{\lambda}\right)\sin(\theta)$, where 2θ is the angle between the incident and scattered beam, and λ is the wavelength of the X-ray. Kapton tape was used as window material in SAXS/WAXS experiments due to its low X-ray absorption and low scattering. The cellulose beads adhere to the Kapton tape surface and are prevented from sliding when the sample holder is placed in a vertical position. Individual 2D scattering patterns of both SAXS and WAXS were collected for 30 and 15 s for drying water swollen and ethanol swollen beads. After radial integration, the background scattering of Kapton tape was scaled and subtracted for each curve to obtain more accurate data. Scaling was completed to account for the change in X-ray transmission that occurs from bead shrinkage during drying.

ASSOCIATED CONTENT

Supporting Information

The Supporting Information is available free of charge at https://pubs.acs.org/doi/10.1021/acsnano.0c00171.

Further details related to the modeling of SAXS data, transparency of beads during drying, drying curves under different conditions, Porod exponent α and β, and SAXS curves for cellulose solution, wet beads, and dry beads (PDF)

AUTHOR INFORMATION

Corresponding Authors

Hailong Li − *Department of Fibre and Polymer Technology, KTH Royal Institute of Technology, SE-100 44 Stockholm, Sweden;* orcid.org/0000-0002-0974-9638; Email: haili@kth.se

Lars Wågberg − *Department of Fibre and Polymer Technology and Wallenberg Wood Science Centre, School of Engineering Sciences in Chemistry, Biotechnology and Health, KTH Royal Institute of Technology, SE-100 44 Stockholm, Sweden;* orcid.org/0000-0001-8622-0386; Email: wagberg@kth.se

Authors

Margarita Kruteva − *Jülich Centre for Neutron Scattering and Biological Matter (JCNS-1/IBI-8), Forschungszentrum Jülich GmbH, D-52425 Jülich, Germany;* orcid.org/0000-0002-7686-0934

Katarzyna Mystek − *Department of Fibre and Polymer Technology, KTH Royal Institute of Technology, SE-100 44 Stockholm, Sweden*

Martin Dulle − *Jülich Centre for Neutron Scattering and Biological Matter (JCNS-1/IBI-8), Forschungszentrum Jülich GmbH, D-52425 Jülich, Germany*

Wenhai Ji − *Jülich Centre for Neutron Science JCNS (JCNS-2), Forschungszentrum Jülich GmbH, D-52425 Jülich, Germany*

Torbjörn Pettersson − *Department of Fibre and Polymer Technology and Wallenberg Wood Science Centre, School of Engineering Sciences in Chemistry, Biotechnology and Health, KTH Royal Institute of Technology, SE-100 44 Stockholm, Sweden;* orcid.org/0000-0002-5444-7276

Complete contact information is available at: https://pubs.acs.org/10.1021/acsnano.0c00171

Notes

The authors declare no competing financial interest.

ACKNOWLEDGMENTS

H.L. acknowledges the ForMAX preproject by the Swedish Ministry of Enterprise and Innovation for funding. L.W. acknowledges the Wallenberg Wood Science Centre at KTH for financial support.

REFERENCES

(1) Postek, M. T.; Vladár, A.; Dagata, J.; Farkas, N.; Ming, B.; Wagner, R.; Raman, A.; Moon, R. J.; Sabo, R.; Wegner, T. H.; Beecher, J. Development of the Metrology and Imaging of Cellulose Nanocrystals. *Meas. Sci. Technol.* **2011**, *22*, No. 024005.

(2) Moon, R. J.; Martini, A.; Nairn, J.; Simonsen, J.; Youngblood, J. Cellulose Nanomaterials Review: Structure, Properties and Nanocomposites. *Chem. Soc. Rev.* **2011**, *40*, 3941–3994.

(3) Perepelkin, K. Lyocell Fibres Based on Direct Dissolution of Cellulose in *N*-Methylmorpholine N-Oxide: Development and Prospects. *Fibre Chem.* **2007**, *39*, 163–172.

(4) Müller, B.; Gebert-Germ, M.; Russler, A. Viscont HT—The Future of High Performance Viscose Filaments and Their Textile Applications. *Lenzinger Ber.* **2012**, *90*, 64−71.
(5) Qi, H.; Chang, C.; Zhang, L. Properties and Applications of Biodegradable Transparent and Photoluminescent Cellulose Films Prepared *via* a Green Process. *Green Chem.* **2009**, *11*, 177−184.
(6) Qi, H.; Cai, J.; Zhang, L.; Kuga, S. Properties of Films Composed of Cellulose Nanowhiskers and a Cellulose Matrix Regenerated from Alkali/Urea Solution. *Biomacromolecules* **2009**, *10*, 1597−1602.
(7) Yang, Q.; Fukuzumi, H.; Saito, T.; Isogai, A.; Zhang, L. Transparent Cellulose Films with High Gas Barrier Properties Fabricated from Aqueous Alkali/Urea Solutions. *Biomacromolecules* **2011**, *12*, 2766−2771.
(8) Chang, C.; Zhang, L. Cellulose-Based Hydrogels: Present Status and Application Prospects. *Carbohydr. Polym.* **2011**, *84*, 40−53.
(9) Gindl, W.; Emsenhuber, G.; Maier, G.; Keckes, J. Cellulose in Never-Dried Gel Oriented by an AC Electric Field. *Biomacromolecules* **2009**, *10*, 1315−1318.
(10) Cai, J.; Kimura, S.; Wada, M.; Kuga, S.; Zhang, L. Cellulose Aerogels from Aqueous Alkali Hydroxide−Urea Solution. *ChemSusChem* **2008**, *1*, 149−154.
(11) Gericke, M.; Trygg, J.; Fardim, P. Functional Cellulose Beads: Preparation, Characterization, and Applications. *Chem. Rev.* **2013**, *113*, 4812−4836.
(12) Wang, S.; Lu, A.; Zhang, L. Recent Advances in Regenerated Cellulose Materials. *Prog. Polym. Sci.* **2016**, *53*, 169−206.
(13) Liebert, T. In *Cellulose Solvents: for Analysis, Shaping and Chemical Modification*; Liebert, T., Heinze, T., Edgar, K. J., Eds.; American Chemical Society: Washington, DC, 2010; pp 3−54.
(14) Cai, J.; Zhang, L.; Zhou, J.; Qi, H.; Chen, H.; Kondo, T.; Chen, X.; Chu, B. Multifilament Fibers Based on Dissolution of Cellulose in NaOH/Urea Aqueous Solution: Structure and Properties. *Adv. Mater.* **2007**, *19*, 821−825.
(15) McCormick, C. L.; Callais, P. A.; Hutchinson, B. H., Jr Solution Studies of Cellulose in Lithium Chloride and *N,N*-Dimethylacetamide. *Macromolecules* **1985**, *18*, 2394−2401.
(16) Kennedy, J.; Rivera, Z.; White, C.; Lloyd, L.; Warner, F. Molecular Weight Characterization of Underivatized Cellulose by GPC using Lithium Chloride-Dimethylacetamide Solvent System. *Cell. Chem. Technol.* **1990**, *24*, 319−325.
(17) Striegel, A. Theory and Applications of DMAc/LiCl in the Analysis of Polysaccharides. *Carbohydr. Polym.* **1997**, *34*, 267−274.
(18) Morgenstern, B.; Kammer, H.; Berger, W.; Skrabal, P. ^{7}Li-NMR Study on Cellulose/LiCl/*N,N*-Dimethylacetamide Solutions. *Acta Polym.* **1992**, *43*, 356−357.
(19) Zhang, C.; Liu, R.; Xiang, J.; Kang, H.; Liu, Z.; Huang, Y. Dissolution Mechanism of Cellulose in *N,N*-Dimethylacetamide/Lithium Chloride: Revisiting through Molecular Interactions. *J. Phys. Chem. B* **2014**, *118*, 9507−9514.
(20) Dawsey, T.; McCormick, C. L. The Lithium Chloride/Dimethylacetamide Solvent for Cellulose: A Literature Review. *J. Macromol. Sci., Polym. Rev.* **1990**, *30*, 405−440.
(21) Lindman, B.; Karlström, G.; Stigsson, L. On the Mechanism of Dissolution of Cellulose. *J. Mol. Liq.* **2010**, *156*, 76−81.
(22) Jones, A. O.; Resel, R.; Schrode, B.; Machado-Charry, E.; Röthel, C.; Kunert, B.; Salzmann, I.; Kontturi, E.; Reishofer, D.; Spirk, S. Structural Order in Cellulose Thin Films Prepared from a Trimethylsilyl Precursor. *Biomacromolecules* **2020**, *21*, 653−659.
(23) Ehmann, H. M.; Werzer, O.; Pachmajer, S.; Mohan, T.; Amenitsch, H.; Resel, R.; Kornherr, A.; Stana-Kleinschek, K.; Kontturi, E.; Spirk, S. Surface-Sensitive Approach to Interpreting Supramolecular Rearrangements in Cellulose by Synchrotron Grazing Incidence Small-Angle X-Ray Scattering. *ACS Macro Lett.* **2015**, *4*, 713−716.
(24) Mohan, T.; Spirk, S.; Kargl, R.; Doliška, A.; Vesel, A.; Salzmann, I.; Resel, R.; Ribitsch, V.; Stana-Kleinschek, K. Exploring the Rearrangement of Amorphous Cellulose Model Thin Films upon Heat Treatment. *Soft Matter* **2012**, *8*, 9807−9815.
(25) Brett, C. J.; Mittal, N.; Ohm, W.; Gensch, M.; Kreuzer, L. P.; Körstgens, V.; Månsson, M.; Frielinghaus, H.; Müller-Buschbaum, P.; Söderberg, L. D.; Roth, S. V. Water-Induced Structural Rearrangements on the Nanoscale in Ultrathin Nanocellulose Films. *Macromolecules* **2019**, *52*, 4721−4728.
(26) Ohm, W.; Rothkirch, A.; Pandit, P.; Körstgens, V.; Müller-Buschbaum, P.; Rojas, R.; Yu, S.; Brett, C. J.; Söderberg, D. L.; Roth, S. V. Morphological Properties of Airbrush Spray-Deposited Enzymatic Cellulose Thin Films. *J. Coat. Technol. Res.* **2018**, *15*, 759−769.
(27) Carrick, C.; Pendergraph, S. A.; Wågberg, L. Nanometer Smooth, Macroscopic Spherical Cellulose Probes for Contact Adhesion Measurements. *ACS Appl. Mater. Interfaces* **2014**, *6*, 20928−20935.
(28) Karlsson, R.-M. P.; Larsson, P. T.; Yu, S.; Pendergraph, S. A.; Pettersson, T.; Hellwig, J.; Wågberg, L. Carbohydrate Gel Beads as Model Probes for Quantifying Non-Ionic and Ionic Contributions behind the Swelling of Delignified Plant Fibers. *J. Colloid Interface Sci.* **2018**, *519*, 119−129.
(29) Karlsson, R.-M. P.; Larsson, P. T.; Hansson, P.; Wågberg, L. The Thermodynamics of the Water-Retaining Properties of Cellulose-Based Networks. *Biomacromolecules* **2019**, *20*, 1603−1612.
(30) Träger, A.; Klein, G.; Carrick, C.; Pettersson, T.; Johansson, M.; Wågberg, L.; Pendergraph, S. A.; Carlmark, A. Macroscopic Cellulose Probes for the Measurement of Polymer Grafted Surfaces. *Cellulose* **2019**, *26*, 1467−1477.
(31) Stuart, M. A.; Huck, W. T.; Genzer, J.; Muller, M.; Ober, C.; Stamm, M.; Sukhorukov, G. B.; Szleifer, I.; Tsukruk, V. V.; Urban, M.; Winnik, F.; Zauscher, S.; Luzinov, I.; Minko, S. Emerging Applications of Stimuli-Responsive Polymer Materials. *Nat. Mater.* **2010**, *9*, 101−113.
(32) Brown, A. C.; Stabenfeldt, S. E.; Ahn, B.; Hannan, R. T.; Dhada, K. S.; Herman, E. S.; Stefanelli, V.; Guzzetta, N.; Alexeev, A.; Lam, W. A.; Lyon, L. A.; Barker, T. H. Ultrasoft Microgels Displaying Emergent Platelet-Like Behaviours. *Nat. Mater.* **2014**, *13*, 1108−1114.
(33) Lu, Y.; Ballauff, M. Thermosensitive Core−Shell Microgels: From Colloidal Model Systems to Nanoreactors. *Prog. Polym. Sci.* **2011**, *36*, 767−792.
(34) Bischofberger, I.; Calzolari, D. C.; De Los Rios, P.; Jelezarov, I.; Trappe, V. Hydrophobic Hydration of Poly-*N*-Isopropyl Acrylamide: A Matter of the Mean Energetic State of Water. *Sci. Rep.* **2015**, *4*, 4377.
(35) Yang, M.; Zhao, K. Cononsolvency of Poly(*N*-Isopropylacrylamide) in Methanol Aqueous Solution-Insight by Dielectric Spectroscopy. *J. Polym. Sci., Part B: Polym. Phys.* **2017**, *55*, 1227−1234.
(36) Maccarrone, S.; Ghavami, A.; Holderer, O.; Scherzinger, C.; Lindner, P.; Richtering, W.; Richter, D.; Winkler, R. G. Dynamic Structure Factor of Core−Shell Microgels: A Neutron Scattering and Mesoscale Hydrodynamic Simulation Study. *Macromolecules* **2016**, *49*, 3608−3618.
(37) Maccarrone, S.; Scherzinger, C.; Holderer, O.; Lindner, P.; Sharp, M.; Richtering, W.; Richter, D. Cononsolvency Effects on the Structure and Dynamics of Microgels. *Macromolecules* **2014**, *47*, 5982−5988.
(38) Stieger, M.; Pedersen, J. S.; Lindner, P.; Richtering, W. Are Thermoresponsive Microgels Model Systems for Concentrated Colloidal Suspensions? A Rheology and Small-Angle Neutron Scattering Study. *Langmuir* **2004**, *20*, 7283−7292.
(39) Stieger, M.; Richtering, W.; Pedersen, J. S.; Lindner, P. Small-Angle Neutron Scattering Study of Structural Changes in Temperature Sensitive Microgel Colloids. *J. Chem. Phys.* **2004**, *120*, 6197−6206.
(40) Berndt, I.; Pedersen, J. S.; Richtering, W. Temperature-Sensitive Core−Shell Microgel Particles with Dense Shell. *Angew. Chem.* **2006**, *118*, 1769−1773.
(41) Keidel, R.; Ghavami, A.; Lugo, D. M.; Lotze, G.; Virtanen, O.; Beumers, P.; Pedersen, J. S.; Bardow, A.; Winkler, R. G.; Richtering, W. Time-Resolved Structural Evolution during the Collapse of

https://dx.doi.org/10.1021/acsnano.0c00171
ACS Nano 2020, 14, 6774−6784

Responsive Hydrogels: The Microgel-To-Particle Transition. *Sci. Adv.* **2018**, *4*, No. eaao7086.
(42) Loxley, A.; Vincent, B. Equilibrium and Kinetic Aspects of the pH-Dependent Swelling of poly (2-Vinylpyridine-Co-Styrene) Microgels. *Colloid Polym. Sci.* **1997**, *275*, 1108−1114.
(43) Dupin, D.; Rosselgong, J.; Armes, S. P.; Routh, A. F. Swelling Kinetics for a pH-Induced Latex-To-Microgel Transition. *Langmuir* **2007**, *23*, 4035−4041.
(44) Bradley, M.; Ramos, J.; Vincent, B. Equilibrium and Kinetic Aspects of the Uptake of Poly (ethylene Oxide) by Copolymer Microgel Particles of *N*-Isopropylacrylamide and Acrylic Acid. *Langmuir* **2005**, *21*, 1209−1215.
(45) Xing, S.; Guan, Y.; Zhang, Y. Kinetics of Glucose-Induced Swelling of P (NIPAM-AAPBA) Microgels. *Macromolecules* **2011**, *44*, 4479−4486.
(46) Saunders, B. R.; Vincent, B. Thermal and Osmotic Deswelling of Poly (NIPAM) Microgel Particles. *J. Chem. Soc., Faraday Trans.* **1996**, *92*, 3385−3389.
(47) Yin, J.; Dupin, D.; Li, J.; Armes, S. P.; Liu, S. pH-Induced Deswelling Kinetics of Sterically Stabilized Poly (2-Vinylpyridine) Microgels Probed by Stopped-Flow Light Scattering. *Langmuir* **2008**, *24*, 9334−9340.
(48) Niebuur, B.-J.; Chiappisi, L.; Zhang, X.; Jung, F.; Schulte, A.; Papadakis, C. M. Formation and Growth of Mesoglobules in Aqueous Poly(*N*-Isopropylacrylamide) Solutions Revealed with Kinetic Small-Angle Neutron Scattering and Fast Pressure Jumps. *ACS Macro Lett.* **2018**, *7*, 1155−1160.
(49) Liu, Y.; Stoeckel, D.; Gordeyeva, K.; Agthe, M.; Schütz, C.; Fall, A. B.; Bergström, L. Nanoscale Assembly of Cellulose Nanocrystals during Drying and Redispersion. *ACS Macro Lett.* **2018**, *7*, 172−177.
(50) Wang, B.; Huang, L. X.; Mujumdar, A. S. Drying of Nanosize Products. In *Handbook of Industrial Drying*; Mujumdar, A. S., Ed.; CRC Press: Boca Raton, FL, 2006; pp 738−753.
(51) Hammouda, B. A New Guinier−Porod Model. *J. Appl. Crystallogr.* **2010**, *43*, 716−719.
(52) Ishii, D.; Tatsumi, D.; Matsumoto, T.; Murata, K.; Hayashi, H.; Yoshitani, H. Investigation of the Structure of Cellulose in LiCl/DMAc Solution and Its Gelation Behavior by Small-Angle X-Ray Scattering Measurements. *Macromol. Biosci.* **2006**, *6*, 293−300.
(53) Aono, H.; Tatsumi, D.; Matsumoto, T. Scaling Analysis of Cotton Cellulose/LiCl·DMAc Solution Using Light Scattering and Rheological Measurements. *J. Polym. Sci., Part B: Polym. Phys.* **2006**, *44*, 2155−2160.
(54) Hura, G.; Sorenson, J. M.; Glaeser, R. M.; Head-Gordon, T. A High-Quality X-Ray Scattering Experiment on Liquid Water at Ambient Conditions. *J. Chem. Phys.* **2000**, *113*, 9140−9148.
(55) K Mahadeva, S.; Yeol Yang, S.; Kim, J. Effects of Solvent Systems on Its Structure, Properties and Electromechanical Behavior of Cellulose Electro-Active Paper. *Curr. Org. Chem.* **2013**, *17*, 83−88.
(56) Liu, Z.; Sun, X.; Hao, M.; Huang, C.; Xue, Z.; Mu, T. Preparation and Characterization of Regenerated Cellulose from Ionic Liquid Using Different Methods. *Carbohydr. Polym.* **2015**, *117*, 99−105.
(57) Wada, M.; Ike, M.; Tokuyasu, K. Enzymatic Hydrolysis of Cellulose I is Greatly Accelerated *via* Its Conversion to the Cellulose II Hydrate Form. *Polym. Degrad. Stab.* **2010**, *95*, 543−548.
(58) Kobayashi, K.; Kimura, S.; Togawa, E.; Wada, M. Crystal Transition from Cellulose II Hydrate to Cellulose II. *Carbohydr. Polym.* **2011**, *86*, 975−981.
(59) Isogai, A.; Usuda, M.; Kato, T.; Uryu, T.; Atalla, R. H. Solid-State CP/MAS Carbon-13 NMR Study of Cellulose Polymorphs. *Macromolecules* **1989**, *22*, 3168−3172.
(60) Sèbe, G.; Ham-Pichavant, F. d. r.; Ibarboure, E.; Koffi, A. L. C.; Tingaut, P. Supramolecular Structure Characterization of Cellulose II Nanowhiskers Produced by Acid Hydrolysis of Cellulose I Substrates. *Biomacromolecules* **2012**, *13*, 570−578.
(61) Tomšič, M.; Jamnik, A.; Fritz-Popovski, G.; Glatter, O.; Vlček, L. Structural Properties of Pure Simple Alcohols from Ethanol, Propanol, Butanol, Pentanol, to Hexanol: Comparing Monte Carlo Simulations with Experimental SAXS Data. *J. Phys. Chem. B* **2007**, *111*, 1738−1751.
(62) Seidell, A. In *Solubilities of Inorganic and Organic Compounds: A Compilation of Quantitative Solubility Data from the Periodical Literature. Supplement to the Third ed. Containing Data Published during the Years 1939−1949 Inclusive;* Seidell, A., Linke, W. F., Francis, A. W., Bates, R. G., Eds.; Van Nostrand: New York, 1952; pp 334−337.
(63) Bertrand, T.; Peixinho, J.; Mukhopadhyay, S.; MacMinn, C. W. Dynamics of Swelling and Drying in a Spherical Gel. *Phys. Rev. Appl.* **2016**, *6*, No. 064010.
(64) Hirosawa, K.; Fujii, K.; Hashimoto, K.; Shibayama, M. Solvated Structure of Cellulose in a Phosphonate-Based Ionic Liquid. *Macromolecules* **2017**, *50*, 6509−6517.
(65) Livsey, I. Neutron Scattering from Concentric Cylinders. Intraparticle Interference Function and Radius of Gyration. *J. Chem. Soc., Faraday Trans. 2* **1987**, *83*, 1445−1452.
(66) Larsson, P. T.; Svensson, A.; Wågberg, L. A New, Robust Method for Measuring Average Fibre Wall Pore Sizes in Cellulose I Rich Plant Fibre Walls. *Cellulose* **2013**, *20*, 623−631.
(67) Carrick, C.; Ruda, M.; Pettersson, B.; Larsson, P. T.; Wågberg, L. Hollow Cellulose Capsules from CO2 Saturated Cellulose Solutions—Their Preparation and Characterization. *RSC Adv.* **2013**, *3*, 2462−2469.
(68) Berthold, F.; Gustafsson, K.; Berggren, R.; Sjöholm, E.; Lindström, M. Dissolution of Softwood Kraft pulps by Direct Derivatization in Lithium Chloride/*N,N*-Dimethylacetamide. *J. Appl. Polym. Sci.* **2004**, *94*, 424−431.

https://dx.doi.org/10.1021/acsnano.0c00171
ACS Nano 2020, 14, 6774−6784